frontiers | Frontiers in Earth Science

ORIGINAL RESEARCH
published: 15 June 2022
doi: 10.3389/feart.2022.872620

Effects of Seawater Recharge on the Formation of Geothermal Resources in Coastal Areas and Their Mechanisms: A Case Study of Xiamen City, Fujian Province, China

Chunlei Liu[1,2], *Yasong Li*[1,2], *Shengwei Cao*[1,2], *Wanli Wang*[1] *and Jing Li*[3]*

[1]*The Institute of Hydrogeology and Environmental Geology, Chinese Academy of Geological Science, Shijiazhuang, China,* [2]*Fujian Provincial Key Laboratory of Water Cycling and Eco-Geological Processes, Xiamen, China,* [3]*Faculty of Environment, China University of Geosciences, Wuhan, China*

The southeast coastal areas of China have abundant geothermal resources. Most especially, seawater-recharged geothermal systems in the coastal areas have large quantiles of recharge but suffer water salinization and low water temperature. Moreover, the geothermal water development in these areas may induce seawater intrusion. Understanding the genetic patterns of geothermal resources is significant for rational exploration and protection. This study analyzed the hydrochemical and environmental isotopic characteristics of geothermal water, groundwater, and surface water samples collected in the area with geothermal resources in Xiamen Province in the southeast coastal areas of China. Based on this, the recharge of geothermal water circulation and the genetic patterns of geothermal resources were revealed. The results of this study indicate that the geothermal water in mountainous areas and piedmonts in Xiamen is mainly recharged by rainfall infiltration. In contrast, the geothermal water in coastal areas in Xiamen is recharged by seawater mixing to different extents, as indicated by hydrochemical types, isotopic characteristics, and the C1-/Br- ratio of geothermal water. As revealed by the calculation results using the Cl^- mixing model, 10 of 13 geothermal fields in Xiamen are recharged by seawater mixing, with a mixing ratio of up to 73.20% in the Pubian geothermal field. After being recharged by rainfall in the low mountainous areas, geothermal water migrates toward deep parts along NW-trending faults. Then, it converges with regional NE-trending deep faults to absorb heat conducted from deep parts to form deep geothermal reservoirs. The deep geothermal reservoirs were estimated to be 185–225°C using the silica-enthalpy mixing model. The geothermal water is mixed with cold water or seawater while rising along faults. The temperature of shallow geothermal reservoirs was estimated to be 71–145°C using SiO_2 geothermometers.

Keywords: geothermal water, environmental isotope, geochemical geothermometer, seawater recharge, genesis of geothermal resources

OPEN ACCESS

Edited by:
Dawei Hu,
(CAS), China

Reviewed by:
Walter D'Alessandro,
National Institute of Geophysics and Volcanology, Section of Palermo, Italy
Kunal Singh,
Geological Survey of India, India

***Correspondence:**
Jing Li
lijing915@cug.edu.cn

Specialty section:
This article was submitted to Geochemistry, a section of the journal Frontiers in Earth Science

Received: *09 February 2022*
Accepted: *23 May 2022*
Published: *15 June 2022*

Citation:
Liu C, Li Y, Cao S, Wang W and Li J (2022) Effects of Seawater Recharge on the Formation of Geothermal Resources in Coastal Areas and Their Mechanisms: A Case Study of Xiamen City, Fujian Province, China. Front. Earth Sci. 10:872620. doi: 10.3389/feart.2022.872620

1 INTRODUCTION

Geothermal resources are new green energy resources that integrate heat, water, and minerals. They are rich and cause low-level environmental pollution compared to fossil energy resources. However, geothermal water with high salinity and high concentrations of As, Hg, F, and H_2S also poses risks of environmental pollution (Giggenbach, 1988; Ozgener and Kocer, 2004; Armienta et al., 2014). In the southeast coastal areas of China, which are in great demand for energy resources, the development and utilization of geothermal energy is an important measure for promoting sustainable urban development (Lin, 2007; Lin et al., 2016; Lin et al., 2020). The hydrothermal systems in southeast coastal areas of China circulate as follows. Faults develop in the low-permeability granite basement, and the atmospheric precipitation is heated through deep circulation in these faults and then rises to the Earth surface (Han and Zhuang, 1988; Hu and Xiong, 1990; Xiong et al., 1990; Liao, 2012; Gan, 2017; Gan et al., 2020). However, geothermal water in some coastal areas in Southeast China shows noticeable salinization and is rich in heavy isotopes, indicating the recharge by seawater mixing (Gao et al., 2009; Wang, 2018). Any changes in interactions between groundwater and seawater—the primary recharge factors of geothermal systems in coastal areas—will directly affect the quantity and quality of geothermal resources in coastal areas. The increase in mixed seawater may lead to a significant increase in the salinization and a decrease in the temperature of the geothermal water. By contrast, the decrease in the mixed seawater may lead to the depletion of geothermal resources. In this case, the exploitation of large amounts of geothermal water may cause the high salinization of geothermal water and seawater intrusion. The depletion and water quality deterioration of geothermal resources induced by the exploration of geothermal reservoirs in the southeast coastal areas of China can be effectively prevented by studying the formation conditions of seawater-recharged hot water systems and the genetic patterns of geothermal water and deeply understanding the formation and evolutionary patterns of low-medium temperature convective geothermal systems in these areas.

Southeast coastal areas are among the geothermal active areas with the most considerable potential for the development and utilization of geothermal resources in South China. These areas have widely distributed Mesozoic volcanic rocks and granites (Xiong et al., 1991; Zhang et al., 2018; Lin, 2022), abundant regional geothermal resources, and a ternary heat accumulation pattern consisting of the radioactive heat production by acidic rocks, heat transfer by faults, and heat retention by cap rocks (Li et al., 2020). Geothermal anomalous areas in southeast coastal areas are all located in low-lying areas such as intermountain basins, stream valleys, and plains. As indicated by the characteristics of the geothermal field in the geothermal anomalous areas, as well as the features of pores in strata, rock joints, and tectonic fractures (Qiu, 2018), the geothermal fields in the Southeast coastal areas lie at the intersections of NNW- and NE/NEE-trending faults (Han and Zhuang, 1988; Fan et al., 1993; Zhang et al., 2020). Among them, the NE -trending faults are major regional geothermal-controlling structures, while NEE- and EW-trending tensional faults serve as major regional water-conducting structures (Ma et al., 2021). As calculated using no-steam loss quartz thermometers, the hot springs in Zhangzhou-Xiamen areas have geothermal reservoir temperatures of 106–149°C and circulation depths of approximately 3400–5100 m (Lin et al., 2020). The recharge and salinization of geothermal water in coastal areas have always been controversial. The chemical and isotopic studies show that, in the Zhangzhou area, which is adjacent to the study area, the atmospheric precipitation mixes with seawater in the deep parts of geothermal fields, leading to a significant increase in the salinity of geothermal water and accordingly the formation of saline water (Pang, 1987). Existing studies are mainly focused on the genesis of geothermal resources from the regional structures and hydrochemical isotopic characteristics of geothermal fields and the estimation of geothermal reservoir temperature. However, few studies have been conducted on the genesis of geothermal sources and the recharge, runoff, and discharge conditions of geothermal fluids. Most especially, the contribution of seawater recharge to the formation of geothermal resources is yet to be ascertained. This study revealed the recharge mechanisms of geothermal water circulation and the genetic patterns of geothermal resources and will assist in effectively preventing and controlling the resource and environment problems such as geothermal water salinization, seawater intrusion, and the decrease in the geothermal water caused by geothermal water exploration and utilization.

2 REGIONAL GEOLOGICAL BACKGROUND

The study area lies in the coastal area in southeastern Fujian Province. It has a subtropical monsoon climate, with an average annual temperature of 20.8°C, an extreme maximum temperature of 38.4°C, and average annual rainfall of 1347.8 mm. Xiamen City lies at the eastern margin of the Cathaysia block of the South China Plate and in the zone where the southeastern margin of the Eurasian Plate interacts with the Pacific Plate (Wang et al., 1993). Because of the intensive and frequent Yanshanian magmatic activities, polyphasic rock masses were formed and widely distributed in the study area. Moreover, the Late Jurassic magmatic activities occurred on the largest scale among the Yanshanian magmatic activities. As a result, highly radioactive acidic Late-Jurassic and Early-Cretaceous granites are widely developed in the study area (Wang et al., 1996). Because of the large-scale Yanshanian magmatic activities, the deep Zhenghe-Dapu Fault Zone and the coastal deep Dongshan Island—Nan'ao Island Fault Zone extend from hundreds of kilometers to more than 1000 km in the NE and NNE directions. They have a long history of multi-stage orogenic activities and are increasingly active in areas closer to the coast (Wang, 1985). The movement of the Philippine Plate in the NW direction caused these deep faults to slide leftward or suffer compression and torsion, leading to the formation of a

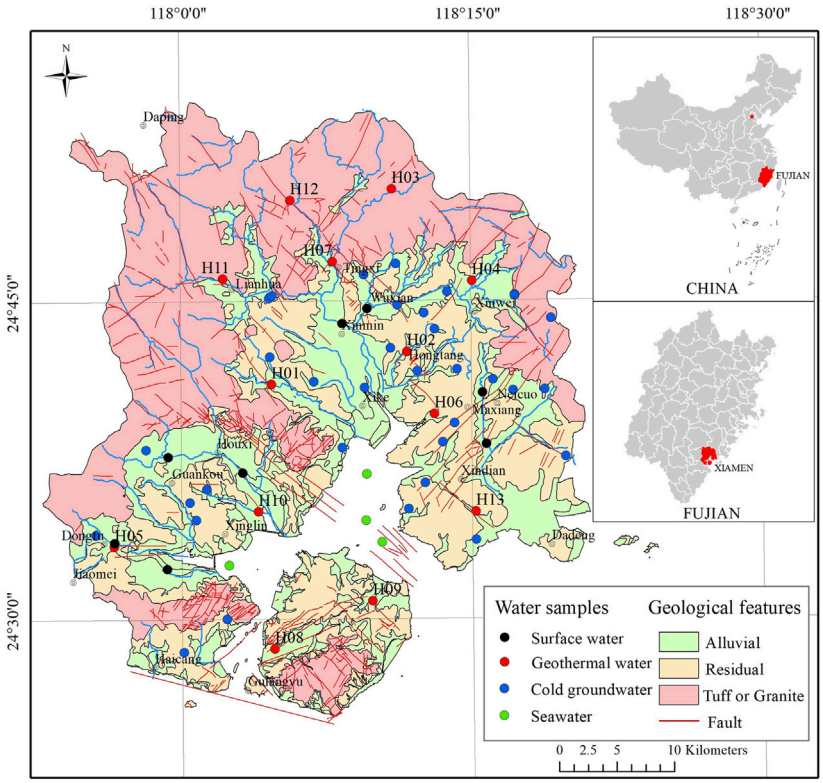

FIGURE 1 | Geological sketch of Xiamen and the distribution of sampling points.

set of tensional or transtensional faults in the NW direction (**Figure 1**).

The study area shows sporadic hydrogeological units, most of which are independent or semi-independent. The groundwater in these hydrogeological units is mainly recharged by atmospheric precipitation and discharges into the sea through short runoff. It can be divided into water in loose-rock porous rocks, water in mesh fractures of weathered zones, and water in bedrock fractures. The former two types of water are primarily distributed in shallow alluvial-diluvial and weathered eluvial strata. The water in bedrock fractures mainly occurs in joints and tectonic cracks in Yanshanian granites and Jurassic volcanic rocks.

3 SAMPLE COLLECTING AND TESTING

Thirteen water samples were collected from geothermal wells with depths of 48.6–500.8 m in the study area. Thirty-four water samples were collected from cold groundwater along the runoff direction of groundwater in the hydrological units of geothermal wells, including 26 samples of water in loose porous rocks (corresponding well depth: 3–25 m) and eight samples of water in bedrock fractures (corresponding well depth: 31–120 m). In addition, eight surface water samples were collected from rivers in the main recharge and discharge areas of groundwater and four samples were collected from seawater (**Figure 1**). The water temperature, pH, and electrical conductivity were measured on-site using the portable Eureka Manta2 water quality recorder. Water samples were stored in clean polyethylene bottles after being filtered using Millipore membrane filters with a pore size of 0.45 μm. Then, they were tested for anions, cations, and hydrogen and oxygen isotopes at the Key Laboratory of Groundwater Science and Engineering, Ministry of Natural Resources. Cations and anions SO_4^{2-} and Br^- were tested using the ICP-OES spectrometer (iCAP-6300) and the Dionex ICS-1500 ion chromatography system, respectively, with testing accuracy of 1% and charge-balance error of 5% or less. Anion Cl^- was tested using the titrimetric method, and SiO_2 was tested using UV-2550 spectrophotometer according to the silicon molybdenum yellow spectrophotometry. Using the method of wavelength-scanned optical cavity ring-down spectroscopy, hydrogen and oxygen isotopes were detected at a temperature of 22°C and relative humidity of 40% with the Picarro L2130-i isotope analyzer. The detection accuracy was 0.2‰ for δ18O and 2‰ for δ^2H. The testing results are shown in **Table 1**.

4 RESULTS AND ANALYSE

4.1 Hydrochemical Characteristics

The temperature of the hot water exposed in the study area is 37.6–88.9°C, and that of the cold groundwater in the area is 23.4–26.8°C. The pH of the geothermal water and surface water

TABLE 1 | List of hydrochemical characteristics of groundwater in Xiamen.

No.	Type	Well depth	T	pH	TDS	K^+	Na^+	Ca^{2+}	Mg^{2+}	Cl^-	SO_4^{2-}	HCO_3^-	CO_3^{2-}	Br^-	SiO_2	δ^2H	$\delta^{18}O$
		m	(°C)		(ppm)	(ppm)	(ppm)	(ppm)	(ppm)	(ppm)	(ppm)	(ppm)	(ppm)	(ppm)	(ppm)	(‰)	(‰)
G01	Cold Groundwater	3.0	26.2	7.02	550	46.3	33.3	96.8	11.1	34	70.3	285	0	<0.10	34.5	−33	−5.4
G02	Cold Groundwater	10.0	24.5	6.4	433	7.06	52	50.1	17.4	61.3	35.2	121	0	<0.10	29	−41	−6.5
G03	Cold Groundwater	44.0	25.4	6.78	248	4.68	14.3	59.6	4.15	17.5	31.5	170	0	<0.10	23.3	−33	−5.1
G04	Cold Groundwater	24.0	25.9	5.88	179	12.9	27.7	11.5	2.48	38.4	20.7	17.7	0	<0.10	28.3	−42	−6.4
G05	Cold Groundwater	11.0	24.6	4.55	222	0.86	27.1	31.3	3.83	40.3	14.1	6.07	0	<0.10	7.81	−38	−5.9
G06	Cold Groundwater	10.0	24.7	7.14	132	1.28	10.7	25.7	2.22	8.73	14.6	88.5	0	<0.10	19.6	−33	−4.7
G07	Cold Groundwater	10.0	24.8	5.35	174	3.2	19.6	21.8	4.06	30.5	9.36	18.2	0	<0.10	14.1	−38	−5.9
G08	Cold Groundwater	10.0	25.9	7.41	555	2.01	64.2	113	13.5	89.3	80.2	309	0	<0.10	22.3	−32	−5.2
G09	Cold Groundwater	38.0	26.8	6.72	98.3	3.75	9.33	4.46	0.92	5.24	3.13	30.5	0	<0.10	49.2	−42	−6.5
G10	Cold Groundwater	10.0	25.7	5.5	181	3.22	11.8	29.3	4.1	15.8	1.91	54.6	0	<0.10	20.6	−43	−6.6
G11	Cold Groundwater	25.0	25.9	6.17	71.5	4.44	9.48	4.08	0.3	8.73	2.47	18.3	0	<0.10	17.7	−34	−5.3
G12	Cold Groundwater	25.0	25.4	6.82	422	5.47	45.5	74.7	8.04	64.8	32.8	150	0	<0.10	11.9	−36	−5.6
G13	Cold Groundwater	13.0	25.1	6.28	244	29.3	36.7	18.4	2.44	41.9	48.3	55.5	0	<0.10	19.2	−37	−5.8
G14	Cold Groundwater	10.0	24.8	6.31	324	52.9	41.3	18.3	3.25	47.9	57.4	30.5	0	<0.10	4.42	−39	−5.9
G15	Cold Groundwater	9.5	25.5	5.86	107	6.04	12	7.98	1.09	15.4	4.87	24.3	0	<0.10	26	−37	−5.8
G16	Cold Groundwater	9.5	26.1	5.79	84	3.53	7.36	9.35	1.43	12.6	4.09	6.07	0	<0.10	10.4	−40	−6.1
G18	Cold Groundwater	9.0	25	6.61	399	4.32	33.6	69.8	9.25	51	38.2	101	0	<0.10	19	−35	−5.6
G19	Cold Groundwater	31.0	25.8	6.35	348	6.78	60.7	30.1	7.15	102	17.9	48.8	0	<0.10	40.2	−39	−6.1
G20	Cold Groundwater	11.3	25.9	7.08	306	7.88	36.1	45.9	4.39	46.5	41.9	82.4	0	<0.10	21.6	−34	−5.3
G21	Cold Groundwater	9.5	24.5	7.51	366	15.6	47.6	41.1	9.12	59.4	28.5	97.6	0	<0.10	25.9	−38	−5.9
G22	Cold Groundwater	10.0	25.6	7.67	132	5.74	17	6.02	1.63	16.1	3.52	31.7	0	<0.10	47.6	−42	−6.4
G23	Cold Groundwater	15.0	24.5	5.35	236	1.98	47.1	17.7	3.24	61.8	12.5	7.32	0	<0.10	13.2	−42	−6.5
G24	Cold Groundwater	11.0	25.4	7.59	414	26.6	44.6	51.1	9.45	60.4	35.1	98.9	0	<0.10	22	−40	−6.2
G26	Cold Groundwater	10.0	25.9	6.71	279	10.7	33.5	44	3.48	40.2	33.2	99.5	0	<0.10	11.1	−33	−5.2
G27	Cold Groundwater	8.0	25.7	6.88	708	4.96	86.5	131	14.7	114	87.9	250	0	<0.10	7.77	−36	−5.6
G28	Cold Groundwater	11.2	24.7	6.42	339	18.3	36.3	39.6	11.9	40.9	56.1	104	0	<0.10	20.3	−32	−5.2
G29	Cold Groundwater	14.4	24.8	6.3	344	2.53	47.3	37.5	15.2	64.6	54.6	64.1	0	<0.10	12.3	−39	−6.1
G30	Cold Groundwater	100.0	24.3	7.23	249	1.37	22.5	49	5.3	8.03	8.46	190	0	<0.10	52.1	−42	−6.3
G31	Cold Groundwater	120.0	25	6.9	186	2.39	17.3	29.3	4.06	9.43	6.48	122	0	<0.10	45.4	−43	−6.5
G32	Cold Groundwater	105.0	25.2	7.36	172	0.96	14.5	32.2	3.6	4.89	13.9	122	0	1.73	36.4	−47	−7.3
G33	Cold Groundwater	100.0	23.4	7.51	171	0.85	14.8	32.2	3.49	4.89	14.5	122	0	<0.10	36.4	−46	−7.2

(Continued on following page)

TABLE 1 | (*Continued*) List of hydrochemical characteristics of groundwater in Xiamen.

No.	Type	Well depth	T	pH	TDS	K^+	Na^+	Ca^{2+}	Mg^{2+}	Cl^-	SO_4^{2-}	HCO_3^-	CO_3^{2-}	Br^-	SiO_2	δ^2H	$\delta^{18}O$
		m	(°C)		(ppm)	(ppm)	(ppm)	(ppm)	(ppm)	(ppm)	(ppm)	(ppm)	(ppm)	(ppm)	(ppm)	(‰)	(‰)
G34	Cold Groundwater	100.0	25.1	7.92	251	0.71	58.6	25.8	0.54	21.7	33.5	140	0	<0.10	37.9	−47	−7
H01	Geothermal water	200.4	56.8	7.34	2300	15.9	619	237	0.71	1210	130	33.6	0	3.94	64.1	−48	−7.3
H02	Geothermal water	140.0	51.7	7.36	1100	8.62	332	53.9	0.23	459	108	104	0	1.17	75.4	−43	−6.4
H03	Geothermal water	48.6	48	8.91	301	1.36	85.2	2.84	0.08	14.7	55.8	73.2	18	<0.10	73.2	−51	−7.7
H04	Geothermal water	110.0	37.6	8.07	326	1.71	86	16.4	0.47	56.6	69	88.5	0	<0.10	49.3	−43	−6.5
H05	Geothermal water	150.6	80	7.11	3640	33.4	828	496	1.3	1950	216	48.8	0	6.4	83.4	−42	−6.2
H06	Geothermal water	151.1	47	6.92	8000	59.9	1830	1060	4.17	4630	297	36.6	0	16.5	84.7	−40	−5.9
H07	Geothermal water	160.0	45.5	7.82	391	2.81	112	14.8	0.26	52.4	73.8	142	0	<0.10	56.3	−43	−6.4
H08	Geothermal water	202.0	38.2	6.94	19300	86.4	4040	2940	185	11100	866	45.8	0	35.3	65.9	−29	−4.2
H09	Geothermal water	150.0	53.6	6.65	17600	127	4320	1870	118	10400	609	84.8	0	38.7	79.1	−29	−4.2
H10	Geothermal water	500.8	88.9	6.86	13800	95.3	3520	1410	129	7550	690	67.1	0	27	107	−32	−4.8
H11	Geothermal water	151.5	47.5	8.68	345	1.43	101	4.4	0.35	16.8	101	55.5	18	<0.10	65.3	−49	−7.5
H12	Geothermal water	51.8	48.5	7.17	443	5.72	99.2	16.2	1.9	11.2	136	110	0	<0.10	114	−47	−7
H13	Geothermal water	151.0	68.3	6.5	21100	201	4650	2810	54.9	12500	447	48.8	0	49.2	98.9	−26	−3.8
S01	Surface Water	-	33.1	8.24	279	12.5	36.5	43.1	5.38	40.9	44.8	140	0	<0.10	19.3	−37	−5.7
S02	Surface Water	-	34.9	9.41	1100	14	147	99.1	2.78	321	49.6	85.4	0	0.92	27.9	−36	−5.3
S03	Surface Water	-	30.7	7.4	121	5.73	11.6	18	2.38	11.9	11	73.2	0	0.12	21	−37	−5.7
S04	Surface Water	-	34.7	7.89	330	12.6	64.6	34.8	7.92	88.7	39.6	122	0	<0.10	16.1	−36	−5.5
S05	Surface Water	-	34.1	7.8	94.9	4.07	9.08	12	1.38	6.99	8.5	48.8	0	<0.10	20.5	−41	−6.4
S06	Surface Water	-	32.6	8.04	147	6.37	15.5	19.8	2.84	17.8	17	61	0	<0.10	20.7	−37	−5.9
S07	Surface Water	-	33.4	9.03	359	14.2	48.9	50.8	7.36	70.6	43.2	177	0	<0.10	27.3	−33	−4.9
S08	Surface Water	-	33.8	8.73	386	14.2	58.8	47.2	7.07	69.2	45	201	0	<0.10	33.4	−32	−4.8
SW01	Seawater	-	28.1	7.86	31300	385	9910	353	1140	17200	2330	138	0	55.7	2.92	-	-
SW02	Seawater	-	28.8	7.87	32700	386	10100	369	1190	17400	2390	133	0	57.3	2.43	-	-
SW03	Seawater	-	31.7	8.2	32400	385	10000	351	1170	17800	2480	134	0	59.2	<1.00	-	-
SW04	Seawater	-	28.5	7.8	29800	352	9330	336	1100	16000	2230	132	0	53.1	3.58	-	-

is 6.50–8.68 and 7.4–9.41, respectively, indicating slightly alkaline water. The pH of the groundwater is 4.55–7.92, suggesting neutral and meta-acidic water.

The salinity of the geothermal water tends to increase from the surrounding mountainous areas to the coastal areas in Xiamen. It is 300–443 mg/L for geothermal water exposed in mountainous and piedmont alluvial-diluvial plains (i.e., samples H03, H04, H07, H11, and H12), 1100–3640 mg/L for those exposed to groundwater runoff areas of alluvial-diluvial plains and eroded platforms (i.e., samples H01, H02, and H05), and 8000–21000 mg/L for those exposed in sea-land intersections (i.e., samples H06, H08, H09, H10, and H13).

According to the Piper trilinear diagram of water samples (**Figure 2**), the cations and anions in the surface water mainly include Ca^{2+}, Na^+, and HCO^{3-}. For the cold groundwater, the cations and anions are dominated by Na^+, Ca^{2+}, HCO^{3-}, and Cl^- and the hydrochemical types mainly include Ca•Na-HCO_3 and Ca•Na-HCO_3•Cl. For the geothermal water in the hilly mountainous areas and the piedmont alluvial-diluvial plains, the cations and anions mainly include Na^+, Ca^{2+}, HCO^{3-}, and SO_4^{2}, and the hydrochemical types are dominated by Ca•Na-HCO_3•SO_4. For the geothermal water in the coastal areas, the cations and anions are dominated by Na^+ and Cl^-, respectively, with the water type of Na-Cl, and the hydrochemical types feature abrupt changes.

Cl^- is not liable to form mineral salts nor is absorbed on mineral surfaces in natural water-rock systems. Moreover, it is hardly affected by water-rock interactions even in a high-temperature environment. Therefore, Cl^- is frequently used to trace the origins of materials in geothermal water and its systems that are closely correlated with Cl^- (Cartwright et al., 2004; Arnórsson and Andrésdóttir, 1995). In the study area, there is a negative correlation between SiO_2 and Cl^- in cold groundwater and the geothermal water H03, H04, H07, H11, and H12 in the

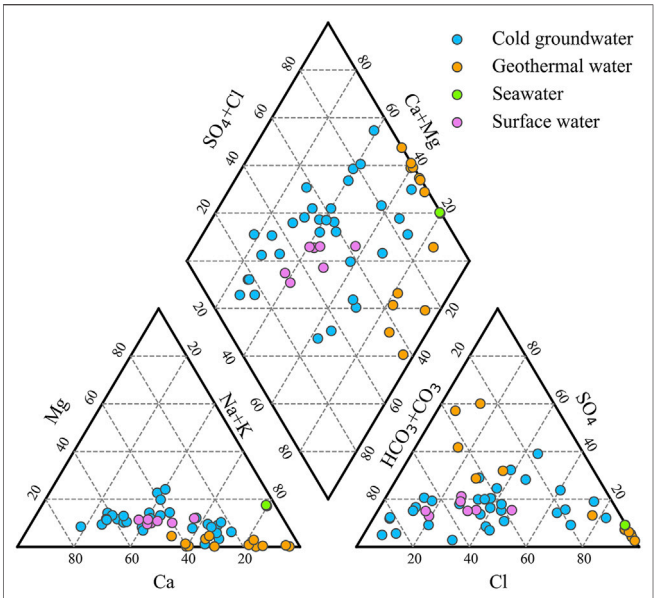

FIGURE 2 | Piper trilinear diagram of water samples from Xiamen.

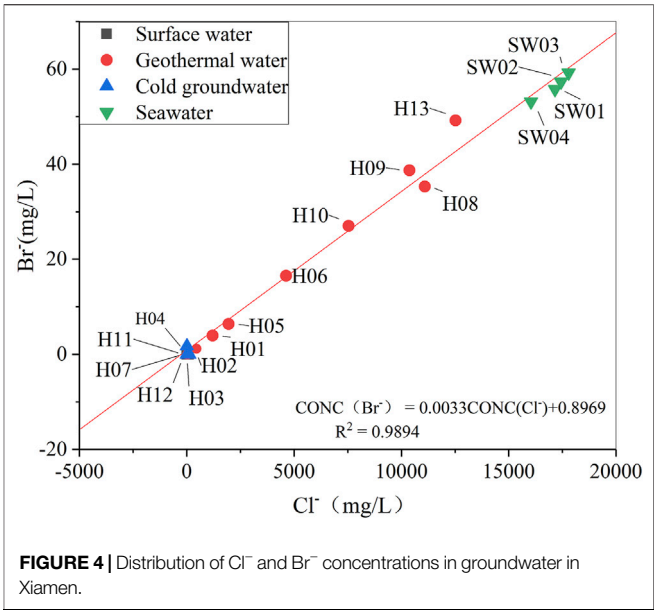

FIGURE 4 | Distribution of Cl^- and Br^- concentrations in groundwater in Xiamen.

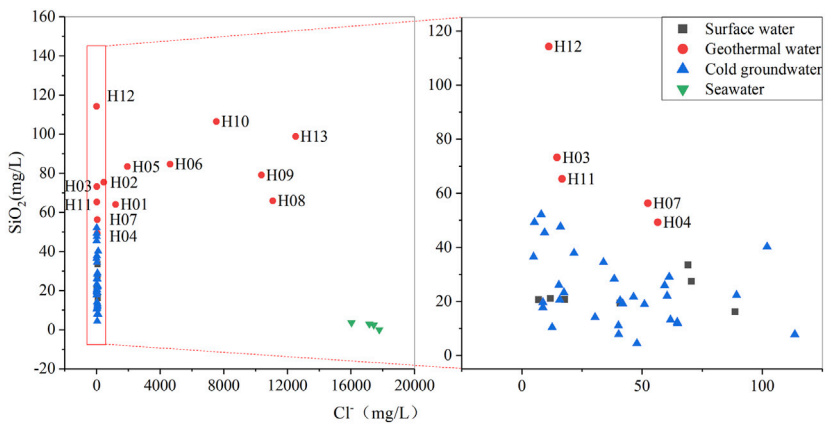

FIGURE 3 | Distribution of SiO_2 and Cl^- concentrations in groundwater in Xiamen.

hilly mountainous areas and piedmont alluvial-diluvial plains, while there is no close correlation between SiO_2 and Cl^- in the nearshore geothermal water (**Figure 3**). These phenomena indicate that the SiO_2 and Cl^- concentrations in the cold groundwater and the geothermal water in the hilly mountainous areas and piedmont plains are controlled by water-rock interactions, while the SiO_2 and Cl^- concentrations in nearshore geothermal water are possibly mainly affected by seawater infiltration (Wang et al., 1986).

4.2 Mixing Ratio of Seawater in Geothermal Water

The Piper trilinear diagram and the isotopic characteristics of groundwater all indicate that the nearshore geothermal water in Xiamen is affected by seawater. **Figure 4** illustrates the Cl^- and Br^- concentrations in the geothermal water. The Br^- concentration of the groundwater in the study area is relatively low and is mostly below the detection limit, while that in the nearshore geothermal water is relatively high. The linear relationship between Cl^- and Br^- concentrations reveals that the salinity of the geothermal water originates from seawater and is controlled by the quantity of mixed seawater. The mixing ratio of seawater in the geothermal water was calculated based on the Cl^- concentration in geothermal water (**Table 2**). Specifically, the Cl^- concentration in seawater was taken as 17100 mg/L, which was the average Cl^- concentration of seawater samples collected from the local sea in Xiamen City. Meanwhile, the Cl^- concentration in geothermal water before seawater mixing was taken as 17.90 mg/L, which was the average Cl^- concentration in

TABLE 2 | Mixing ratio of seawater in geothermal water in Xiamen.

No.	Landform type	Cl^-(mg/L)	Mixing ratio of seawater %
H03	Bedrock	14.67	0.00
H11		16.77	0.00
H12		11.18	0.00
H01	Alluvial residual plain	1209	6.97
H02		459.3	2.58
H04		56.58	0.23
H07		52.39	0.20
H05		1947	11.29
H06	Alluvial marine floodplain	4628	26.99
H08		11090	64.82
H09		10374	60.63
H10		7545	44.06
H13		12522	73.20

oxygen isotopes of geothermal fields show obvious zonation. Geothermal waters H01, H03, H11, and H12, which are distributed in low mountains, hills, and river valleys, have relatively negative water isotopes and low temperatures due to the recharge of water from high altitude areas. The elevation of the mountain is about 1175 m in the study area. In addition, groundwater could be recharged during the glacial period, contributing to the depleted water isotopes. The ^{14}C ages of waters H06 and H13 are greater than 18 ka. The temperature of geothermal water tends to be higher and the isotopes of geothermal water tend to approximate those of seawater near the coast (Cai, 2003; **Figure 5**). When the seawater has a maximum $\delta^{18}O$ value of −1.29, the $\delta^{18}O$ values at the freshwater endmember of geothermal water were calculated to

TABLE 3 | δ^2H and $\delta^{18}O$ of coastal seawater in Xiamen.

Sample	Sampling timing	$\delta^2H\ V_{SMOW}$ (‰)		$\delta^{18}O_{VSMOW}$ (‰)	
		1998–11-06	1998–12-06	1998–11-06	1998–12-06
Seawater	H	−15.9 ± 0.6	−10.2 ± 0.3	−1.94 ± 0.02	−1.29 ± 0.03
	L	−17.8 ± 0.4	−12 0.6 ± 0.1	−2.35 ± 0.05	−1.53 ± 0.02

"H" denotes high tide and "L" denotes low tide.

groundwater in the bedrock mountainous areas. The calculation results show that the geothermal water H3, H4, H7, H11, and H12 exposed in the piedmont areas is not affected by seawater mixing, while the nearshore geothermal water is affected by seawater mixing at different levels. The geothermal water H13 in the Pubian geothermal field shows the highest mixing ratio of seawater, which is up to 73.20%.

4.3 Environmental Isotopic Characteristics of Groundwater

In the study area, the $\delta^{18}O$ and δ^2H values of hot water are −7.7 to −3.8‰ and −51 to −26‰, respectively, and those of cold water are −7.3 to −4.7‰ and −47 to −32‰, respectively.

The local meteoric water line (LMWL) of Xiamen approximates the global meteoric water line (GMWL; Yurtsever, 1975), with the slope and y-intercept of the former being greater than those of the latter (Chen et al., 2016). The delta values of hydrogen and oxygen isotopes in the surface water, groundwater, and geothermal water in the study area are distributed on both sides of the local atmospheric precipitation line, indicating that the water in the area is mainly recharged by atmospheric precipitation. The seawater in the Xiamen Bay is greatly affected by the Jiulong River with a total annual runoff of 8.22 billion m^3 and the surface water and groundwater surrounding Xiamen. Large amounts of surface water and groundwater mix with seawater in the Xiamen Bay, causing the seawater to be rich in negative water isotopes. As shown by the testing data, the seawater in the Xiamen Bay has $\delta^{18}O$ values of −2.35 to −1.29 and thus is rich in negative water isotopes compared to open ocean water (**Table 3**). The hydrogen and

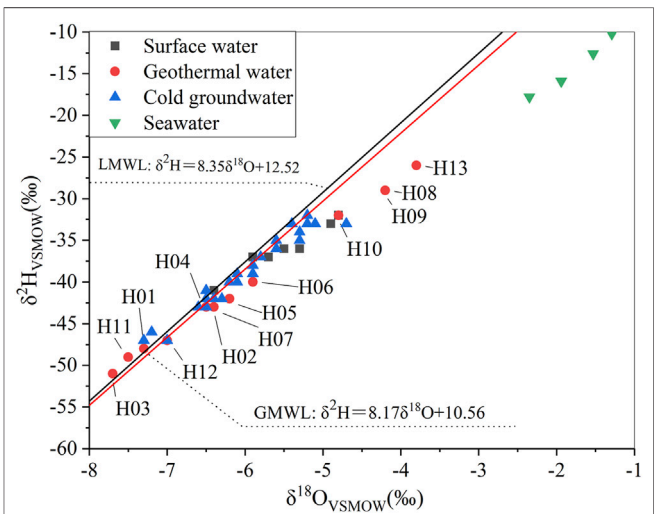

FIGURE 5 | Distribution of stable hydrogen and oxygen isotopes in geothermal water in Xiamen.

be −10.66 to −6.4 (average: −7.7) based on the mixing ratio of seawater. For example, Pubian (H13) is rich in negative water isotopes, with a $\delta^{18}O$ value of −10.66. When the seawater has a minimum $\delta^{18}O$ of −2.35, the calculated $\delta^{18}O$ values at the freshwater endmember of geothermal water were −7.7 to −6.4. The $\delta^{18}O$ values at freshwater endmember of geothermal water approximate to those of the precipitation in the study area, indicating that the freshwater endmember of geothermal water was recharged by atmospheric precipitation. In addition, the

TABLE 4 | Estimated temperatures of geothermal reservoirs in Xiamen.

No.	Temperature of water	Quartz thermometer (°C, no-steam loss)	Chalcedony thermometer (°C)
H01	56.8	114	85
H02	51.7	122	94
H03	48.0	121	92
H04	37.6	101	71
H05	80.0	127	100
H06	47.0	128	100
H07	45.5	107	78
H08	38.2	115	86
H09	53.6	125	97
H10	88.9	141	114
H11	47.5	115	86
H12	48.5	145	119
H13	68.3	137	110

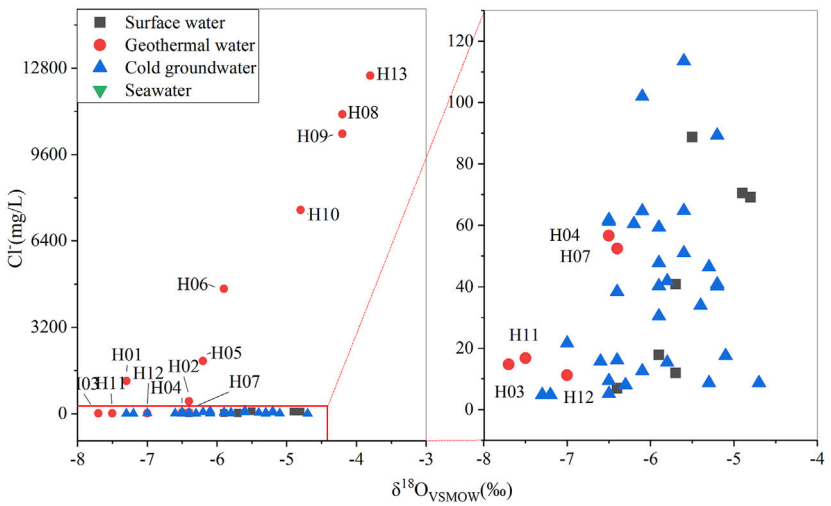

FIGURE 6 | Relationship between the distribution of Cl^- concentration and $\delta^{18}O$.

groundwater in the geothermal water Pubian (H13) has a ^{14}C age of 19.7 ka, indicating that the freshwater endmember of groundwater in the hot spring could be recharged during the glacial period.

According to the relationships between Cl^- concentration and $\delta^{18}O$ values (**Figure 6**), Cl^- is poorly correlated with $\delta^{18}O$ for cold groundwater and the geothermal water in mountainous areas in Xiamen. In contrast, there is a significantly positive correlation between Cl^- and $\delta^{18}O$ for the geothermal water in coastal areas, indicating a marine origin of Cl^- in geothermal water. The geothermal water circulation in offshore areas could be affected by the paleo-seawater trapped in the marine sediments or modern seawater. The regional geological tectonism in Xiamen is dominated by crustal uplift, with merely a small number of thin marine sedimentary strata. In this case, paleo-seawater cannot be stored. Therefore, it can be inferred that the geothermal water in coastal areas in Xiamen is mainly recharged by modern seawater.

5 DISCUSSION

5.1 Water-Rock Equilibrium State

The Na-K-Mg ternary diagram can be used to distinguish different types of water samples based on the equilibrium state of geothermal water (**Figure 7**). The ternary diagram shows three zones, namely the zones of fully equilibrated water, partially equilibrated water, and immature water. It is applied on the basis that K and Na concentrations can reach equilibrium faster than Mg and K concentrations (Giggenbach, 1988). The geothermal water in the study area is partially equilibrated water, except for H04 and H12, which are immature water. The water-rock interactions in the study area have not yet reached the fully equilibrated state, and dissolution still continues. The geothermal water may originate from a hotter environment and is mixed and diluted by shallow cold water during its deep circulation and rise. As a result, the contents of chemical components in hot water change. The high salinity and

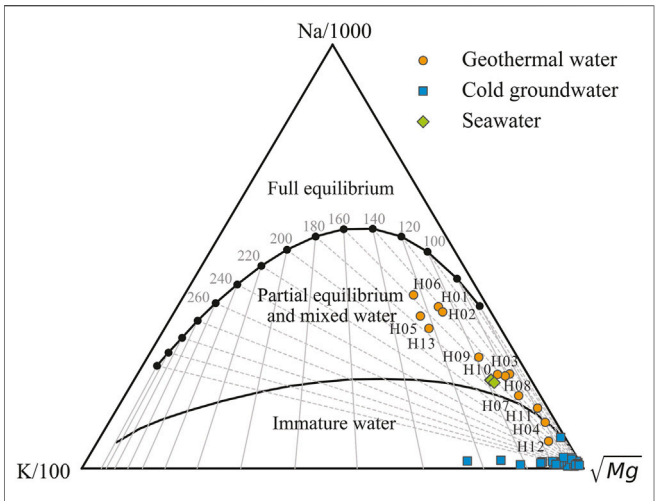

FIGURE 7 | Na-K-Mg ternary diagram of geothermal water samples in Xiamen.

Cl^- concentration of geothermal water originate from seawater mixing, which brings abundant ions such as Na^+ and K^+ besides Cl^-. Meanwhile, the Na-K-Mg ternary diagram shows that all cold groundwater samples lie near the Mg endmember at the lower right corner. This phenomenon indicates that the temperature of water-rock equilibrium is low and Na and K minerals in hot water do not reach equilibrium. The Na/K ratios of the partially equilibrated waters indicate a possible equilibration temperature range of 140–180°C. This result suggests that the high-temperature geothermal water that undergoes deep circulation is mixed with shallow cold water, thus forming partially equilibrated or immature water.

5.2 Estimation of Geothermal Reservoir Temperature

Geochemical geothermometers can be used to calculate the temperature of underground geothermal reservoirs based on the concentrations of chemical components in geothermal water. In the geothermal system, the migration of hot water from deep to shallow parts tends to be accompanied by the dissolution and precipitation reactions of various minerals. If a certain mineral concentration shows a relationship with the fluid temperature when it reaches the reaction equilibrium in the solution, the mineral concentration can be used to deduce the temperature of mineral equilibrium (i.e., the ambient temperature) (Craig, 1953; Li et al., 2022). Geothermal geothermometers generally include SiO_2, gas, isotopic, and cation geothermometers. The cation geothermometers are related to components such as Na, K, and Mg. This study revealed that a large amount of seawater is mixed into the geothermal water in Xiamen. As a result, the concentrations of key cations in the geothermal water have the same orders of magnitude as those in the cold groundwater, making it difficult to conduct correction using the mixing ratio. In other words, the seawater mixing makes the essential application conditions of cation geothermometers unavailable (Fournier, 1977; Fournier and Potter, 1982). SiO_2 geothermometers are devised based on the concentrations of SiO_2 minerals in geothermal water since the solubility of SiO_2 minerals is the function of temperature. Moreover, pressure and the increase in salts (leading to the change in salinity) have small effects on the solubility of quartz and non-crystalline silica when the geothermal reservoir temperature is less than 300°C (Verma and Santoyo, 1997).

Most geothermal water in the study area is partially equilibrated water, and only Dongtang (H04) and Tangli (H12) are immature water. Moreover, geothermal water H01, H02, H05, H06, H07, H08, H09, H10, and H13 is mixed with seawater at different levels. Seawater can enter the geothermal water in the deep or shallow parts. When seawater mixing occurs in deep parts, water-rock interactions reach the equilibrated state after seawater mixing and thus cation geothermometers are applicable. However, in the case of seawater mixing in shallow parts, water-rock interactions have not reached the equilibrated state after seawater mixing and thus cation geothermometers are inapplicable. It is difficult to determine whether seawater enters the geothermal water in the deep or shallow parts using currently available data. Moreover, partially equilibrated water (H03, H11) highly approaches immature water, possibly leading to large errors in the temperature calculated using cation geothermometers.

SiO_2 geothermometers are devised based on the solubility of the SiO_2 minerals including quartz, chalcedony, and amorphous non-crystalline silica (Fournier and Rowe, 1966; Fournier and Truesdell, 1973). At a temperature range of 0–250°C, the results calculated using the formulas of quartz geothermometers are very close to the solubility of quartz under the vapor pressure of solutions (Fournier et al., 1980). Therefore, the calculation results of geothermometers are accurate at this temperature range. However, the geothermal reservoir temperature in the study area is generally less than 250°C as revealed by relevant research results. In general, quartz and chalcedony determine the SiO_2 concentration at temperatures of > 180°C and < 110°C, respectively, but the minerals that control the SiO_2 concentration at a temperature of 110–180°C are still unknown (Arnorsson, 1975). This study selected quartz and chalcedony geothermometers. Quartz geothermometers can be divided into no-steam loss geothermometers and maximum steam loss geothermometers. Since the temperature at geothermal wellheads is significantly lower than the local boiling point, the no-steam loss quartz thermometer and chalcedony geothermometer was used in this study (Fournier, 1977). As revealed by the geothermal temperatures calculated using SiO_2 geothermometers, the quartz geothermometer and the chalcedony geothermometer yielded geothermal reservoir temperatures of 101–145°C, and 71–119°C (**Table 4**).

5.3 Mixing Model

Given that the geothermal water in the study area is mixed with cold water and seawater in shallow parts, this study used the silica-enthalpy mixing model to determine the mixing ratio of hot water with shallow cold water and to obtain the original temperature of the geothermal reservoirs (Fournier and Truesdell,

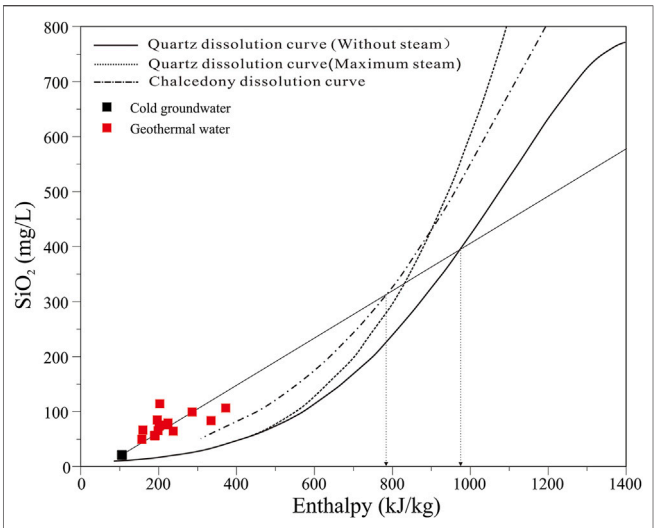

FIGURE 8 | Silica-enthalpy illustration method.

5.4 Formation Mechanisms of Geothermal Resources

The low-medium temperature geothermal systems in the study area are affected by deep mantle-derived materials to a limited extent, and their He isotopic ratios show typical crustal metamorphic characteristics (Tian et al., 2021). The heat in the study area mainly originates from the heat transfer of EW-trending deep faults and the radioactive heat production of granites. The shallow groundwater or seawater surrounding geothermal anomalous areas infiltrates downward along the fractures of NW-trending structures while continuously absorbing heat (heating, expanding, and specific gravity decreasing). When it infiltrates to heat sources, where the geothermal water is about 185–225°C, the pressure difference formed by the temperature difference between the heat sources and their surrounding areas pushes the geothermal water to rise along tensional fractures and then release thermal energy. Meanwhile, the surrounding low-temperature groundwater continuously infiltrates and recharges the geothermal water. As a result, the shallow geothermal reservoirs in the study area have a temperature of 71–149°C. The temperature difference between the heat sources and their surrounding areas continues pushing the geothermal water to constantly rise, leading to the formation of the convective geothermal systems in igneous rock areas in southeast coastal areas of China (**Figure 9**).

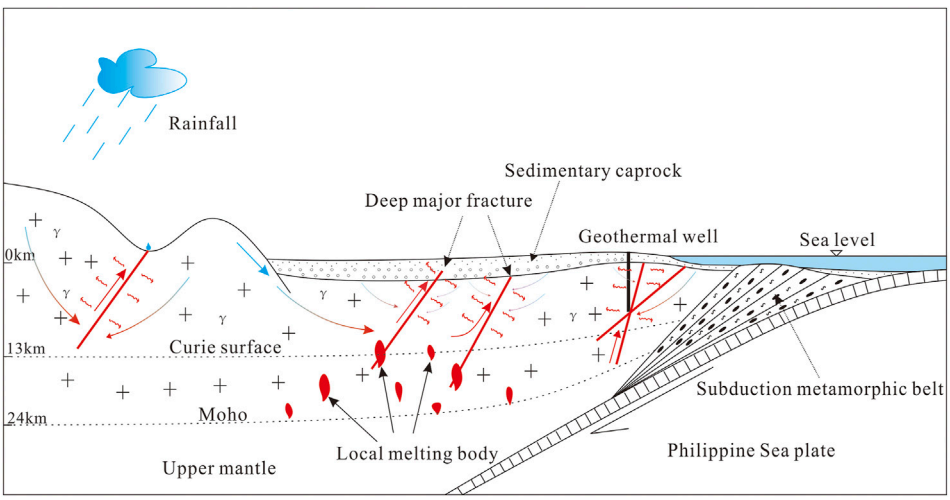

FIGURE 9 | Diagram showing the genetic model of geothermal resources in igneous rock areas in the southeast coastal areas of China.

1973). In this study, the average temperature of cold water samples was used as the cold water endmember (t = 21°C, SiO_2 = 20.64 mg/L). In the silica-enthalpy mixing model, assuming no steam or heat loss, the hot water endmember and the cold water endmember were projected into the silica-enthalpy diagram (**Figure 8**). Then, the temperature range of deep geothermal reservoirs was determined by the temperatures corresponding to three points of intersection of the line passing the hot water points and the cold water point and the solubility curves of quartz and chalcedony (Alcicek et al., 2018), and the mixing ratio range of cold water is the proportions of the distance between the hot water point and the intersection points along the line. Using the silica-enthalpy illustration method, it can be estimated that deep geothermal reservoirs in Xiamen have enthalpy values of 775–975 kJ/kg and temperatures of 185–225°C and that the mixing ratio of cold water is 63–91%.

6 CONCLUSION

The geothermal water exposed in Xiamen has a temperature of 37.60–88.90°C. It is slightly alkaline water, and its hydrochemical types mainly include Ca•Na-HCO_3 and Ca•Na-HCO_3•Cl. From piedmont areas to the coastal areas, the salinity of the geothermal water constantly increases. Moreover, the geothermal water in the

coastal areas has a hydrochemical type of Na-Cl, showing an abrupt change compared with the cold groundwater.

The geothermal water in coastal areas in Xiamen is recharged by seawater mixing to different extents according to the hydrochemical types, isotopic characteristics, and the C1-/Br- ratio of geothermal water. As revealed by the calculation results using the Cl^- mixing model, 10 of 13 geothermal fields in Xiamen are recharged by seawater mixing. The geothermal water in the Pubian geothermal field (H13) shows the highest mixing ratio of seawater, which is up to 73.20%. Furthermore, the freshwater recharge endmember of the deep geothermal water in Xiamen could be recharged during the glacial period.

The geothermal resources in Xiamen mainly have low-medium temperatures. The geothermal fields in piedmont areas are recharged by rainfall infiltration, while those in the coastal areas are recharged by rainfall and seawater mixing. The quartz and chalcedony geothermometers yielded geothermal reservoir temperatures of 101–145°C and 71–119°C, respectively.

The NE-trending faults in Xiamen have significant impacts in deep parts and constitute channels that allow deep heat to rise. The NW- and near-EW-trending faults are mainly tensional and constitute the recharge, runoff, and discharge circulation channels of geothermal water. Atmospheric precipitation infiltrates downward along the NW- and near-EW-trending faults to the NE-trending faults, and groundwater temperature reaches 185–225°C subject to deep heat transfer. The temperature difference results in the pressure difference, which causes the geothermal water to rise along tensional fractures and the surrounding cold water to continuously infiltrate and recharge the geothermal water. As a result, the mixing ratio of cold water is up to 63–91%, and the shallow geothermal reservoirs in Xiamen have temperatures of 71–145°C.

DATA AVAILABILITY STATEMENT

The original contributions presented in the study are included in the article/Supplementary files, further inquiries can be directed to the corresponding author.

AUTHOR CONTRIBUTIONS

All authors listed have made a substantial, direct, and intellectual contribution to the work and approved it for publication. CL: Conceptualization, Writing-original draft, Visualization, Funding acquisition. YL: Methodology, Resources, Project administration. SC: Investigation, Data curation. JL: Formal analysis, Writing-review and editing, Supervision.

FUNDING

This work was supported by China Geological Survey project (DD20190303).

REFERENCES

Alçiçek, H., Bülbül, A., Brogi, A., Liotta, D., Ruggieri, G., Capezzuoli, E., et al. (2018). Origin, Evolution and Geothermometry of the Thermal Waters in the Gölemezli Geothermal Field, Denizli Basin (SW Anatolia, Turkey). *J. Volcanol. Geotherm. Res.* 349, 1–30. doi:10.1016/j.jvolgeores.2017.07.021

Armienta, M. A., Rodriguez, R., Ceniceros, N., Cruz, O., Aguayo, A., and Morales, P. (2014). Groundwater Quality and Geothermal Energy. The Case of Cerro Prieto Geothermal Field, Mexico. *Renewable Energy* 63, 236–254.

Arnórsson, S., and Andrésdóttir, A. (1995). Processes Controlling the Distribution of Boron and Chlorine in Natural Waters in Iceland. *Geochimica Cosmochimica Acta* 59 (20), 4125–4146. doi:10.1016/0016-7037(95)00278-8

Arnorsson, S. (1975). Application of the Silica Geothermometer in Low Temperature Hydrothermal Areas in Iceland. *Am. J. Sci.* 275 (7), 763–784. doi:10.2475/ajs.275.7.763

Cai, M. (2003). The Study of Hydrogen and Oxygen Isotopes of Coastal Groundwater in Xiamen Island. *Mar. Sci.* 27 (9), 1–6. doi:10.3969/j.issn.1000-3096.2003.09.001

Cartwright, I., Weaver, T. R., Fulton, S., Nichol, C., Reid, M., and Cheng, X. (2004). Hydrogeochemical and Isotopic Constraints on the Origins of Dryland Salinity, Murray Basin, Victoria, Australia. *Appl. Geochem.* 19 (8), 1233–1254.

Chen, Y., Du, W., Chen, J., and Xu, L. (2016). Composition of Hydrogen and Oxygen Isotopic of Precipitation and Source Apportionment of Water Vapor in Xiamen Area. *Acta Sci. Circumstantiae* 36 (2), 667–674. doi:10.13671/j.hjkxxb.2015.046410.5846/stxb201408251674

Craig, H. (1953). The Geochemistry of the Stable Carbon Isotopes. *Geochimica Cosmochimica Acta* 3 (2-3), 53–92. doi:10.1016/0016-7037(53)90001-5

Dezi, W., Qijiang, R., Jiansheng, Q., Kerong, C., Zhaowen, X., and Jiahu, Z. (1996). Characteristics of Volcanic Rocks in the Shoshonite Province, Eastern China, and Their Metallogenesis. *Acta Geol. Sin. Ed.* 9 (3), 246–259. doi:10.1111/j.1755-6724.1996.mp9003003.x

Fan, W., Menzies, M. A., Yi, H. X., Chen, X., and Zhou, H. (1993). Nature and Processes of the Lower Lithosphere of the Southeast China Coast. *Geotect. Metallogenia* 17 (1), 27–34.

Fournier, R. O. (1977). Chemical Geothermometers and Mixing Models for Geothermal Systems. *Geothermics* 5 (1-4), 41–50. doi:10.1016/0375-6505(77)90007-4

Fournier, R. O., and Potter, R. W., II (1982). A Revised and Expanded Silica (Quartz) Geothermometer. *Geotherm. Resour. Counc. Bull.* 11 (10), 3–12.

Fournier, R. O., and Rowe, J. J. (1966). Estimation of Underground Temperatures from the Silica Content of Water from Hot Springs and Wet-Steam Wells. *Am. J. Sci.* 264 (9), 685–697. doi:10.2475/ajs.264.9.685

Fournier, R. O., Thompson, J. M., and Austin, C. F. (1980). Interpretation of Chemical Analyses of Waters Collected from Two Geothermal Wells at Coso, California. *J. Geophys. Res.* 85 (B5), 2405–2410. doi:10.1029/JB085iB05p02405

Fournier, R. O., and Truesdell, A. H. (1973). An Empirical NaKCa Geothermometer for Natural Waters. *Geochimica Cosmochimica Acta* 37 (5), 1255–1275. doi:10.1016/0016-7037(73)90060-4

Gan, H., Lin, W., Yan, X., Yue, G., Zhang, W., and Wang, G. (2020). Analysis of Geothermal Occurrence Characteristics and Origin of the Thermal Anomalies in the Hidden Igneous Rock Area in the Central Guangdong. *Acta Geol. Sin.* 94 (7), 2096–2106. doi:10.19762/j.cnki.dizhixuebao.2020215

Gan, H., Lin, W., Yue, G., Wang, X., Ma, F., and Wang, G. (2017). Research on the Fault Controlling Mechanism of Geothermal Water in Zhangzhou Basin. *J. Groundwater Sci. Eng.* 5 (4), 326–335.

Gao, F., Yang, X., Wu, A., Fu, Y., and Chen, Y. (2009). Characteristics of Thermal Springs and Genesis of Thermal Underground Waters in Hainan Island. *J. Jilin Univ.* 39 (2), 281–287. doi:10.3969/j.issn.1671-5888.2009.02.016

Giggenbach, W. F. (1988). Geothermal Solute Equilibria. Derivation of Na-K-Mg-Ca Geoindicators. *Geochimica Cosmochimica Acta* 52 (12), 2749–2765. doi:10.1016/0016-7037(88)90143-3

Han, Q., and Zhuang, Q. (1988). On the Source and Pathway of Hot Water in Zhangzhou Basin, Fujian. *Sci. J. Earth Sci.* 13 (3), 271–277.

Hu, S., and Xiong, L. (1990). Reservoir Modelling of Zhangzhou Low Temperature Fracture Zone System, Fujian, China. *Geol. Sci. Technol. Inf.* 9 (4), 65–71.

Li, J., Zhang, L., Ruan, C., Tian, G., Sagoe, G., and Wang, X. (2022). Estimates of Reservoir Temperatures for Non-magmatic Convective Geothermal Systems: Insights from the Ranwu and Rekeng Geothermal Fields, Western Sichuan Province, China. *J. Hydrology* 609 (3), 127668. doi:10.1016/j.jhydrol.2022.127668

Li, T., lin, W., Gan, H., Yue, G., Zhang, D., and Wang, G. (2020). Research on the Genetic Model and Exploration Progress of Hot Dry Rock Resources on the Southeast Coast of China. *J. Geomechanics* 26 (2), 187–200. doi:10.12090/j.issn.1006-6616.2020.26.02.018

Liao, Z. (2012). Deep-Circulation Hydrothermal Systems without Magmatic Heat Source in Fujian Province. *Geoscience* 26 (1), 85–98. doi:10.3969/j.issn.1000-8527.2012.01.009

Lin, S. (2007). Characteristics, Exploitation and Utilization of Geothermal Resources in the Xinglinwan Area of Xiamen City. *Geol. Fujian* 27 (2), 249–253. doi:10.3969/j.issn.1001-3970.2008.02.021

Lin, W., Chen, X., Gan, H., and Yue, G. (2020). Geothermal, Geological Characteristics and Exploration Direction of Hot Dry Rocks in the Xiamen Bay-Zhangzhou Basin, Southeastern China. *Acta Geol. Sin.* 94 (7), 2066–2077. doi:10.19762/j.cnki.dizhixuebao.2020223

Lin, W., Gan, H., Wang, G., and Ma, F. (2016). Occurrence Prospect of HDR and Target Site Selection Study in Southeastern of China. *Acta Geol. Sin.* 90 (8), 2043–2058. doi:10.3969/j.issn.0001-5717.2016.08.031

Lin, W. J., Wang, G. L., Gan, H. N., Wang, A. D., Yue, G. F., and Long, X. T. (2022). Heat Generation and Accumulation for Hot Dry Rock Resources in the Igneous Rock Distribution Areas of Southeastern China. *Lithosphere* 2021 (5), 2039112. doi:10.2113/2022/2039112

Ma, Z., Ma, Y., Zhang, P., Si, F., Huo, Q., and Chu, L. (2021). Application of Wide Area Electromagnetic Method in Geothermal Exploration of Hongtang Town, Fujian Province. *Mineral. Explor.* 12 (3), 661–667. doi:10.3969/j.issn.1674-7801.2021.03.019

Ozgener, O., and Kocer, G. (2004). Geothermal Energy Utilization in Jordanian Deserts. *Energy Sources* 26 (4), 353–360. doi:10.1080/00908310490424105

Pang, Z. (1987). *Zhangzhou Basin Geothermal System–Genesis Model, Energy Pottential and the Occurrence of Thermal Water*. Beijing: Institute of Geology and Geophysics, 270.

Qiu, Z. (2018). *Study on Geothermal Resources and its Causes in Xiamen*. Beijing: China University of Geosciences.

Tian, J., Li, Y., Zhou, X., Pang, Z., Li, L., Xing, L. Z., et al. (2021). Geochemical Characteristics of Hydrothermal Volatiles from Southeast China and Their Implications on the Tectonic Structure Controlling Heat Convection. *Front. Earth Sci.* 9, 1–13. doi:10.3389/feart.2021.786051

Verma, S. P., and Santoyo, E. (1997). New Improved Equations for Na/K, Na/Li and SiO2 Geothermometers by Outlier Detection and Rejection. *J. Volcanol. Geotherm. Res.* 79 (1-2), 9–23. doi:10.1016/S0377-0273(97)00024-3

Wang, D., Zhang, R., and Shi, Y. (1986). *General Hydrogeology*. Beijing: Geological Publishing House.

Wang, J. (1985). Distributions and Formation of the Geothermal Field along the Coast, Southeastern China. *Seismol. Geol.* 7 (1), 49–58.

Wang, P., Chen, Y., Cao, B., Pan, J., and Wang, C. (1993). Crust-upper Mantle Structure and Deep Structure Setting of Fujian Province. *Geol. Fujian* 12 (2), 79–158.

Wang, X. (2018). *Formation Conditions and Hydrogeochemical Characteristicsof the Geothermal Water in Typical Coastal Geothermal Field with Deep Faults*. Wuhan: Guangdong Province , China University of Geosciences.

Xiong, L., Wang, J., and Pang, Z. (1990). Convective and Conductive Heat Flows in Zhangzhou Geothermal Field, Fujian Province, China. *Chin. J. Geophys.* 33 (6), 702–711. doi:10.1016/0009-2541(90)90098-R

Xiong, S., Jin, D., Sun, K., Zou, Z., Fan, S. Y., Du, B. X., et al. (1991). Some Characteristics of Deep Structure of the Zhangzhou Geothermal Field and It's Neighbourhood in the Fujian Province. *Chin. J. Geophys.* 34 (1), 55–63. doi:10.1007/BF02919155

Yurtsever, Y. (1975). Worldwide Survey of Stable Isotopes in Precipitation. International Report. Vienna: IAEA.

Zhang, J., Wang, B., Tang, X., Dong, M., and Ai, Y. (2018). Temperature Structure and Dynamic Background of Crust and Mantle beneath the High Heat Flow Area of the South China Continental Margin. *Chin. J. Geophys.* 61 (10), 3917–3932. doi:10.6038/cjg2018L0448

Zhang, Y., Luo, J., and Feng, J. (2020). Characteristics of Geothermal Reservoirs and Utilization of Geothermal Resources in the Southeastern Coastal Areas of China. *J. Groundwater Sci. Eng.* 8 (2), 134-142. doi:10.19637/j.cnki.2305-7068.2020.02.005

Conflict of Interest: The authors declare that the research was conducted in the absence of any commercial or financial relationships that could be construed as a potential conflict of interest.

Publisher's Note: All claims expressed in this article are solely those of the authors and do not necessarily represent those of their affiliated organizations, or those of the publisher, the editors and the reviewers. Any product that may be evaluated in this article, or claim that may be made by its manufacturer, is not guaranteed or endorsed by the publisher.